Observation of a different magnetic disorder in $ErCo_2$

Julia Herrero-Albillos,* Fernando Bartolomé, and Luis M. García
Instituto de Ciencia de Materiales de Aragón and Departamento de Física de la Materia Condensada, CSIC-Universidad de Zaragoza, Pedro Cerbuna 12, 50009 Zaragoza, Spain

Anthony T. Young
Advanced Light Source, Lawrence Berkeley National Laboratory, University of California, Berkeley, California 94720, USA

Tobias Funk
UCSF Physics Research Laboratory, 185 Berry Street, San Francisco, California 94107, USA

Javier Campo
Instituto de Ciencia de Materiales de Aragón and Departamento de Física de la Materia Condensada, CSIC-Universidad de Zaragoza, Pedro Cerbuna 12, 50009 Zaragoza, Spain

Gabriel J. Cuello
Institut Laue Langevin, 6, rue Jules Horowitz, Boîte Postale 156, F-38042 Grenoble Cedex 9, France
(Received 15 April 2007; revised manuscript received 17 July 2007; published 14 September 2007)

X-ray magnetic circular dichroism (XMCD), small-angle neutron scattering (SANS), and ac magnetic susceptibility (χ_{ac}) measurements as a function of temperature and magnetic field on the Laves phase compound $ErCo_2$ are presented. The results allow one to investigate in detail the $ErCo_2$ paramagnetic phase. The XMCD data reveal an extended region on the phase diagram where the net magnetization of the Er and Co sublattices are oriented in opposite directions at temperatures well above the ferrimagnetic ordering temperature. The complete characterization of the phenomenon by means of SANS and χ_{ac} measurements allows us to propose the occurrence of short-range magnetic order, which we described and systematically studied and which we denote as parimagnetism. The origin of the parimagnetism is analyzed in terms of the different magnetic interactions present in the system. We conclude that parimagnetism in $ErCo_2$ is driven by the formation of Co magnetic clusters which are ferromagnetically coupled within the paramagnetic phase.

DOI: 10.1103/PhysRevB.76.094409 PACS number(s): 81.30.Bx, 71.20.Lp, 75.20.Hr

I. INTRODUCTION

The physical properties of the RM_2 (R=rare earth, M=transition metal) Laves phases have been intensely studied since the 1960s due to the richness and variety of magnetic behaviors present in these compounds.[1–3] For example, substitution of the transition metal M in these compounds can profoundly affect the magnetic properties. In the RFe_2 compounds, Fe bears an intrinsic magnetic moment, independent of the rare-earth ion. In this series, both Fe and R magnetic moments coexist, giving rise to a rich magnetic phenomenology. In contrast, in RNi_2 compounds, all the magnetism comes from the R sublattice, as Ni d bands are fully occupied. Therefore, RNi_2 is an excellent model system to study the magnetism of localized magnetic moments in metals. The intermediate case is provided by the RCo_2 family, in which the Co $3d$ band is near the critical condition for the formation of magnetic moment. Indeed, the Co band is very sensitive to the internal magnetic field created by the rare-earth sublattice as well as to external parameters such as pressure or applied field.[4–8] In those compounds where R is nonmagnetic, the Co moment requires applying very high magnetic fields [$>$70 T for YCo_2 (Ref. 9)] to be induced, through a metamagnetic transition. On the contrary, in the RCo_2 compounds formed with a magnetic rare earth, the internal field is able to induce and polarize the cobalt moment. RCo_2 is therefore a model system for the study of the magnetism of itinerant electron systems, in particular, of metamagnetic processes.[9–12] More recently, a renewed scientific interest has grown around the Co Laves phases due to the magnitude of the magnetocaloric effect associated with its magnetic ordering[13–17] that makes those compounds showing a first-order transition ($ErCo_2$, $HoCo_2$, and $DyCo_2$) good candidates for applications in magnetic refrigeration at low temperatures.

Due to these interesting properties, the Co Laves phases have been extensively studied in the last decades. However, the nature of the Co moment in the paramagnetic phase of RCo_2 compounds is still under debate. Gignoux *et al.*[18] concluded from their magnetic susceptibility and neutron scattering experiments that there is a small Co induced moment in the paramagnetic phase. In contrast, Burzo[19] assigned an effective moment of $2\mu_B$ to Co in the paramagnetic region from high-temperature magnetic susceptibility measurements. Indeed, whether or not an intrinsic magnetic moment in the Co sublattice exists has been a continuous matter of debate.[5,7,20–27]

Among the RCo_2 compounds, $ErCo_2$ is a particularly interesting one, as the molecular field created by Er moments on the Co sublattice is just above the critical value to induce the metamagnetic transition in the Co moments.[28] Therefore, the Co sublattice is especially sensitive to variations of the external parameters. The magnetic behavior in the ordered state is dominated by the Er sublattice, with an essentially temperature-independent magnetic moment of around

8.8 μ_B/atom.[29] As Er is a heavy rare-earth element, the Co magnetic sublattice is ordered antiparallel to the Er one through a first-order magnetostructural transition at $T_c \simeq 32$ K at zero applied magnetic field.[1,30,31] The nature of the cobalt magnetic moment in the paramagnetic phase of $ErCo_2$ is an especially interesting open question, as discussed in a very recent work by Liu and Altounian.[32] They have predicted theoretically a transition from a low-spin state for Co ($\sim 0.1\ \mu_B$) to the well known high-spin state of the ferrimagnetic phase ($\sim 1\ \mu_B$) at the onset of the ordering temperature of $ErCo_2$. This theoretical prediction has not been experimentally confirmed yet.

The aim of this work is to study the paramagnetic phase of $ErCo_2$ taking advantage of the unique capability of x-ray magnetic circular dichroism (XMCD) to perform specific magnetometry, directly measuring the Er and Co net magnetic moments above and below T_c by probing the $4f$ and $3d$ electrons at the $M_{4,5}$ and the $L_{2,3}$ edges, respectively. Using this technique, we have shown an unusual and rich behavior of the Co magnetic moments in the paramagnetic phase, which we attribute to the formation—well above T_c—of sizeable magnetic short-range correlated regions about each Co moment, which in this paper we shall refer to as *magnetic clusters*. We have confirmed the existence of such clusters and studied its field and temperature dependence by means of small-angle neutron scattering (SANS) and ac susceptibility measurements. Our results offer a picture of the paramagnetic phase in $ErCo_2$, showing a short-range magnetic arrangement of Co and Er moments, which we described and systematically studied.

The paper is organized as follows. We first describe the synthesis and characterization of the samples in Sec. II. Section III describes the experimental results: XMCD, SANS, and ac susceptibility measurements are reported in Secs. III A–III C, respectively. We discuss the whole set of experimental data, leading to the proposal of a magnetic phase diagram of $ErCo_2$ in Sec. IV. Finally, we summarize our results in Sec. V.

II. SAMPLE CHARACTERIZATION

The $ErCo_2$ samples were prepared by melting the high-purity elements (99.9%) in an induction furnace under Ar atmosphere. The resulting polycrystalline ingots were wrapped in tantalum foil and further annealed under Ar atmosphere at 850 °C for a week. Several ingots were synthesized in order to check the reproducibility of the observed phenomena.

X-ray diffraction analysis was performed on powdered samples at room temperature as quality control. Data were collected in the range $20° < 2\theta < 115°$ with a step scan mode of $\Delta 2\theta = 0.03°$. The measurements were performed in a Rigaku RTO 500RC diffractometer with Bragg-Brentano geometry and using Cu $K\alpha$ radiation. Rietveld analysis of the diffractograms was performed using FULLPROF software,[33,34] assuring single-phase samples with good crystallization and cubic $Fd\bar{3}m$ structure. No impurities were detected within the 1% accuracy of powder diffraction methods. The x-ray diffractogram together with the Rietveld refinement of one of the $ErCo_2$ samples can be found in Ref. 35.

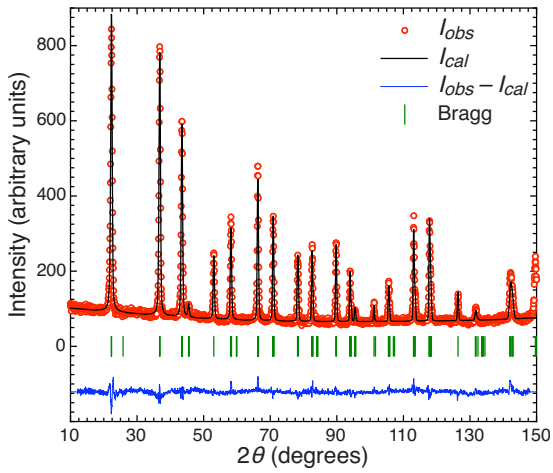

FIG. 1. (Color online) Neutron diffractogram in $ErCo_2$ at 5 K and 0 T. Empty circles and the continuous line are, respectively, the observed and the calculated intensities from the Rietveld refinement including the magnetic contribution. Vertical lines indicate the position of the Bragg peaks and the line at the bottom of the graph shows the difference of the observed and calculated intensities.

Neutron diffraction measurements were also performed in one of the samples at 100, 50, and 5 K. The measurements were performed at the D2B high-resolution diffractometer at Institut Laue Langevin. Data were collected using a wavelength of $\lambda = 1.59$ Å in the range $10° < 2\theta < 150°$ with a step of $\Delta(2\theta) = 0.05°$. The neutron diffractogram for $ErCo_2$ at 5 K is shown in Fig. 1. The Rietveld refinement for this low-temperature diffractogram confirms a ferrimagnetic coupling of Er and Co with magnetic moments of $8.84 \pm 0.06\ \mu_B$ and $0.95 \pm 0.03\ \mu_B$, respectively, with a space group $R\bar{3}m$. This corroborates the well known cubic to rhombohedric distortion occurring in $ErCo_2$ at the magnetic ordering transition. In the ordered phase, the magnetic moments of Er and Co are aligned along the cubic [111] direction.[36]

The samples were also analyzed by scanning electron microscopy. In order to check their homogeneity, energy dispersive spectroscopy was carried out in different areas, confirming a predominant phase with the nominal stoichiometric 1:2 composition. Small amounts of oxides were found at the surface. Very small areas of the samples were found to have a larger amount of Er_2O_3. These rare-earth oxides are antiferromagnetic at very low temperatures ($T < 5$ K) (Ref. 37) and, therefore, do not contribute to the magnetic behavior of our samples at the temperature range of interest.

A complete magnetic characterization from 10 to 300 K was performed in a Quantum Design superconducting quantum interference device (SQUID) magnetometer under applied fields up to 5 T. This study was completed up to 9 T in a Quantum Design extraction magnetometer. The magnetic ordering transition in $ErCo_2$ is coupled to a first-order structural transition, giving rise to abrupt jumps in $M(T)$ and $M(H)$, as well as the expected dependence of the critical temperature T_c with the applied magnetic field H (i.e., $\partial T_c / \partial H > 0$). The experimental $M(T,H)$ surface for $ErCo_2$ is

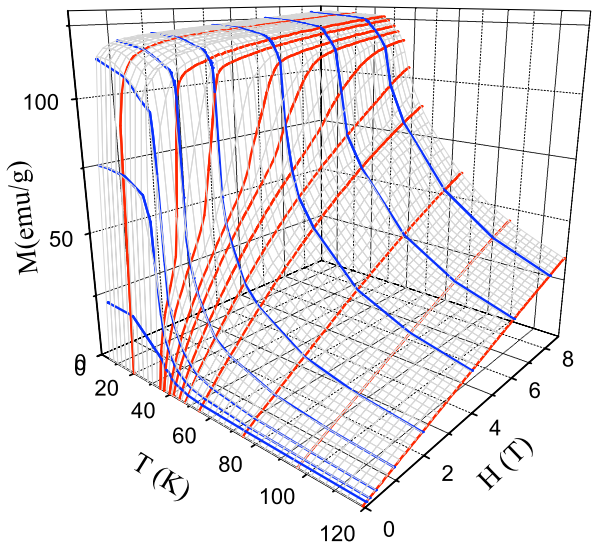

FIG. 2. (Color online) $M(T,H)$ surface of $ErCo_2$ obtained from the isothermal and isofield magnetization curves measured in SQUID and PPMS magnetometers.

shown in Fig. 2, where the cited characteristics of a first-order transition can be observed.

The magnetic and structural characterizations of the samples used in this work are in very good agreement with results from the literature[4,14,15,19,30,38–40] and a comprehensive study of their thermodynamic properties has been already published.[17,35,41]

III. EXPERIMENTAL RESULTS AND DISCUSSION

A. X-ray magnetic circular dichroism

We have measured XMCD at the Co $L_{2,3}$ and Er $M_{4,5}$ absorption edges, -which explore the Co $3d$ and Er $4f$ empty states, respectively, through the magnetic transition and up to temperatures well within the paramagnetic phase. The experiments were carried out at beamline 4.0.2 at Advanced Light Source using a low-temperature end station equipped with a magnet.[42–44] Data were collected at temperatures between 5 and 250 K and with magnetic fields up to 5 T. The detection method used was total electron yield. The samples were freshly cleaved and maintained on Ar atmosphere prior to exposure to x rays in order to avoid surface oxidation.

The XMCD signals are obtained from the difference of two normalized absorption spectra taken with opposite photon helicity under the same applied magnetic field. For the Co $L_{2,3}$ edges, the absorption spectra are normalized so that the step is equal to 1, while the Er $M_{4,5}$ absorption spectra were normalized so that the maximum value of the sum of every two spectra taken with opposite photon helicity is equal to 1. Figure 3 shows some typical XMCD spectra for the Co $L_{2,3}$ edges and Er $M_{4,5}$ edges above and below the ferrimagnetic transition at 1 and 5 T (T_c=34 K and T_c =44 K, respectively). The observed features of the recorded spectra are typical of Co and Er XMCD spectra obtained from metallic systems.[45,46]

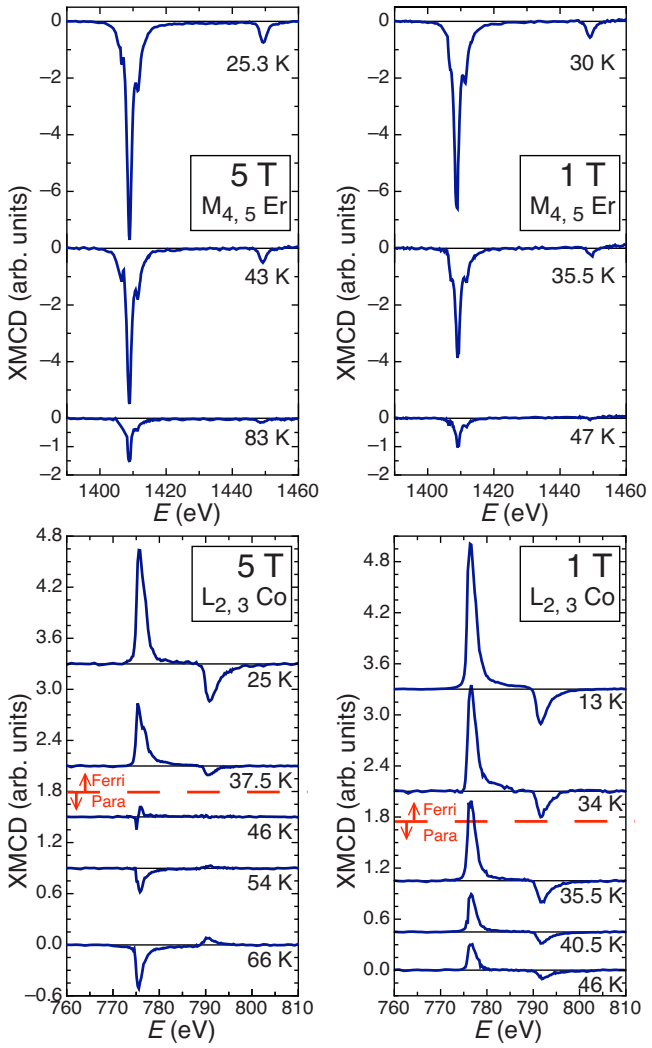

FIG. 3. (Color online) XMCD spectra at the Co $L_{2,3}$ (down) and Er $M_{4,5}$ (up) edges in $ErCo_2$ both below and above the ferrimagnetic transition at H=5 T (left) and H=1 T (right). Dashed line in the Co $L_{2,3}$ edge graphs separates the spectra measured in the ferrimagnetic phase (up) and paramagnetic phase (down).

The signals in the ferrimagnetic phase have been scaled, taking into account the value of Er and Co moments obtained from the Rietveld refinement of the neutron diffractogram. The separate evolution with temperature and applied magnetic field of the Co and Er net magnetic moments can be studied from the XMCD spectra recorded at the Co $L_{2,3}$ and Er $M_{4,5}$ absorption edges. In particular, the area of the XMCD signal at Er M_5 edge is proportional to the magnetization of the Er sublattice[46] and Co magnetization is proportional to $-5A+4B$, where A and B are the areas of the Co XMCD curves at the L_3 and L_2 edges, respectively.[47] Figure 4 shows the magnetization of Er and Co sublattices as a function of temperature at H=1 and 5 T. The total magnetization measured in a SQUID magnetometer is also represented in Fig. 4, showing that, as expected, the sum of the magnetization of the Er and Co sublattices reproduces the total magnetization. Moreover, both Er and Co magnetizations show abrupt jumps at the ordering transition.

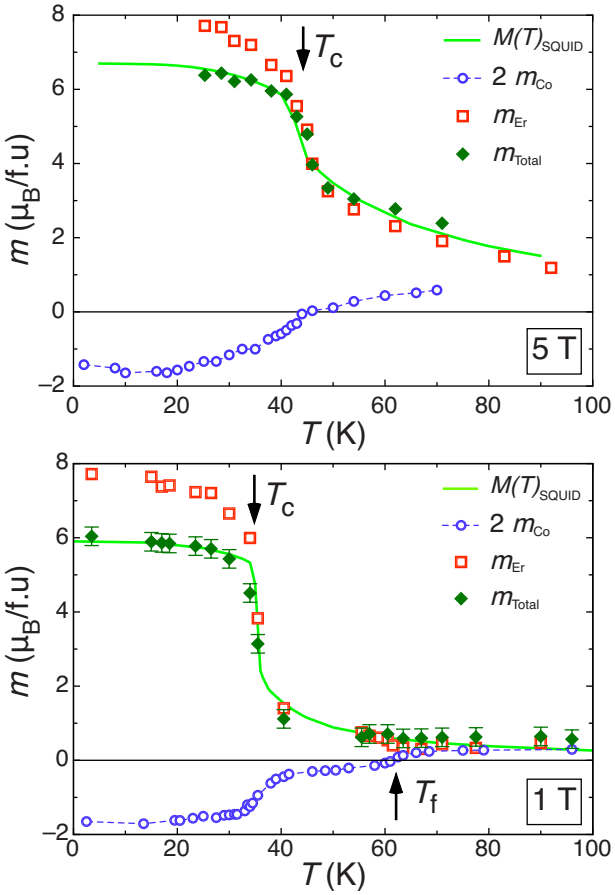

FIG. 4. (Color online) Selective magnetometry in $ErCo_2$ from XMCD measurements: open squares and circles represent the Er and Co net magnetizations per atom, respectively. Full diamonds are the sum of Er and Co magnetizations and the continuous line is the total magnetization measured in a SQUID magnetometer.

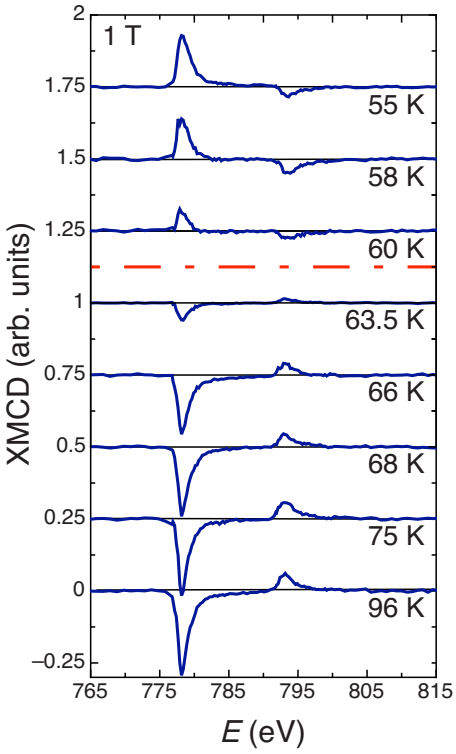

FIG. 5. (Color online) XMCD spectra at the Co $L_{2,3}$ edge in the compound $ErCo_2$ in the vicinity of T_f at $H=1$ T. The dashed line separates the spectra measured above and below T_f.

In $ErCo_2$, the Er magnetic moment is large compared to the Co one and, hence, when a magnetic field is applied, the Er net magnetic moment is parallel to the applied field at all temperatures. Accordingly, the XMCD signal obtained at the Er $M_{4,5}$ absorption edges maintains the same sign at all temperatures and applied fields, with only a decrease in magnitude being observed as the temperature is raised. In contrast, the Co moment behaves in a very unconventional way. First, the presence of a XMCD signal at the Co $L_{2,3}$ edges at all temperatures evidences that Co bears a net magnetic moment also in the paramagnetic phase. At sufficiently high temperatures, as in every paramagnet, the Co magnetic sublattice is polarized parallel to the applied magnetic field. Below T_c, as in a usual ferrimagnet, Co is ordered antiparallel to Er, due to the intersublattice exchange and Hund's third rule. This usual behavior can be observed in the Co $L_{2,3}$ XMCD signal recorded at $H=5$ T, where the signal changes in sign at the ordering transition, $T_c=44$ K (see the lower-left panel in Fig. 3).

Surprisingly, the Co magnetization at $H=1$ T remains opposite to the Er magnetization up to temperatures as high as two times the ordering temperature (see the lower-right panel in Fig. 3 and the lower panel in Fig. 4). In the following, we will denote the temperature at which the Co net magnetization is zero as the flipping temperature, T_f ($T_f=61$ K at $H=1$ T, $T_f=T_c=44$ K at $H=5$ T).

For the measurements at $H=1$ T, the change of sign in the Co magnetization is accompanied by another abrupt jump on the Co magnetization. This flipping of the Co magnetization well above T_c can be better observed in Fig. 5, where some of the Co $L_{2,3}$ edge spectra are shown in the proximity of T_f.

In order to clarify this phenomenon, one has to take into account the real and effective fields acting on the Co moments:

(1) the external applied magnetic field (H_{appl}), which tends to align the Co moments parallel to H_{appl} and therefore also to the Er moments;

(2) the exchange field created by the Er sublattice (H_{Er}), which tends to align the Co moments antiparallel to the Er moments and therefore also to H_{appl};

(3) the exchange field created by the Co sublattice (H_{Co}), which tends to align all the Co moments in the same sense.

The Co magnetization changes its sign with respect to H_{appl} due to the competition between these magnetic fields. The strongest interaction in the system is the Co-Co exchange[20,48–51] but it does not favor any particular direction for the Co sublattice, as it tends to align all the Co moments together, regardless of the direction of H_{Er} and H_{appl}. Therefore, the Co magnetization sign is determined by temperature dependence of H_{Er} and H_{appl}.

(1) At low temperatures—in the ordered phase—the an-

tiferromagnetic exchange interaction between Er and Co dominates, and therefore the Co moments are ordered antiparallel to H_{appl}.

(2) At high temperatures—well above T_c—the Er sublattice magnetization is very small (proportional to its paramagnetic susceptibility and to H_{appl}), and then H_{appl} dominates the Co behavior: the Co moments are disordered but the net Co sublattice magnetization is parallel to H_{appl}.

(3) In the intermediate temperature region, between T_c and T_f (34 and 61 K, respectively, at $H=1$ T), there is no long-range order but, as the XMCD spectra evidence, H_{Er} dominates over H_{appl}, inducing an antiparallel arrangement of the Co and Er net magnetic moments in the paramagnetic phase.

However, a single Co atom would have to overcome H_{Co} to invert the sense of its own magnetic moment. As the Co-Co exchange is the strongest interaction present in the system, the occurrence of T_f in the paramagnetic phase would not be energetically favorable for any value of H_{appl} and H_{Er}. This leads us to propose that the reversal of the Co moments must take place in a collective way, thus minimizing the number of antiparallel Co-Co neighbors.

B. Small-angle neutron scattering

In order to prove the existence of short-range order above T_c in $ErCo_2$ and to study its relationship with the flipping of the Co sublattice, we have performed SANS experiments on $ErCo_2$ in the range of temperatures and fields of interest (magnetic fields between 0.5 and 1 T and temperatures between 5 and 275 K). The SANS measurements were performed at diffractometer D16 at Institut Laue Langevin, using a cryomagnet with vertical field. The detector was placed so that its normal forms an angle of $\gamma=6.23°$ with the neutron beam. The neutron wavelength was $\lambda=4.54$ Å.

The two-dimensional (2D) diffractograms has been analyzed using the GRASP program.[52] The integration of the 2D diffractogram was performed in a 20° circular sector with origin in the neutron beam and in the direction perpendicular to the applied field, where the magnetic contribution is maximum.

In the paramagnetic phase and for the q range explored, only the magnetic contribution originated from the sample (I_m) is temperature and magnetic field dependent. Therefore, it is straightforward to obtain I_m by subtracting from the data a diffractogram measured at a temperature where no magnetic contribution is expected (I_{nm}), i.e., measured at high temperature. We have measured the SANS intensity at 275 K for $H=1$ T and at 113 K for $H=0.5$ T, well above the ferrimagnetic transition and T_f, where it can be reasonably assumed that the magnetic contribution is negligible. The difference between the measured SANS intensity and I_{nm} is the magnetic contribution from the sample I_m.

As a first approximation, I_m can be analyzed using the model-free representation, as shown in Fig. 6,[53–55] where the curves $I_m(T)$ at $H=0.5$ T for selected q values are shown ($q=0.08$, 0.11, 0.15, and 0.21 Å^{-1}). An abrupt change in I_m is observed at T_c for all q's, which is directly ascribed to the divergence of the magnetic correlation length when cooling down to T_c from above and to the change in symmetry already cited in Sec. II. It is interesting to note that Fig. 6 shows that I_m does not drop to zero just above T_c but shows a noticeable high plateau in the SANS intensities and a rather abrupt jump (for low q values) near T_f, providing a clear evidence of the formation of magnetic clusters in the paramagnetic phase of $ErCo_2$ in that region of the phase diagram, well above T_c.

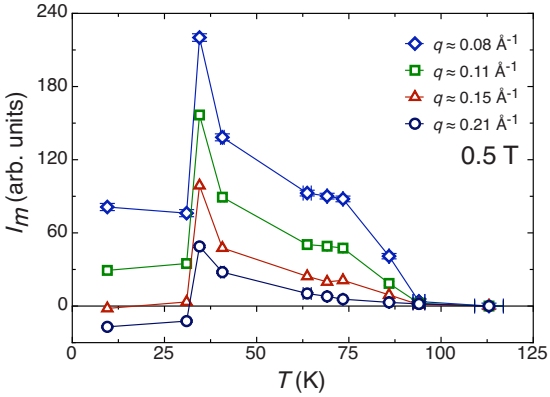

FIG. 6. (Color online) I_m as a function of temperature at selected q values for $ErCo_2$ at an applied magnetic field of 0.5 T.

In order to obtain a quantitative value for the correlation length and its evolution with the temperature and the applied field, it is necessary to assume a model for the magnetic scattering.[54–58] Several models have been tested; however, a linear dependence of $1/I_m$ with q^2 at all the temperatures in the $ErCo_2$ paramagnetic phase is evidenced by the so-called Ornstein-Zernike-Debye plot shown in Fig. 7.[57,59,60] Therefore, $I_m(q)$ is well represented by a Lorentzian function,

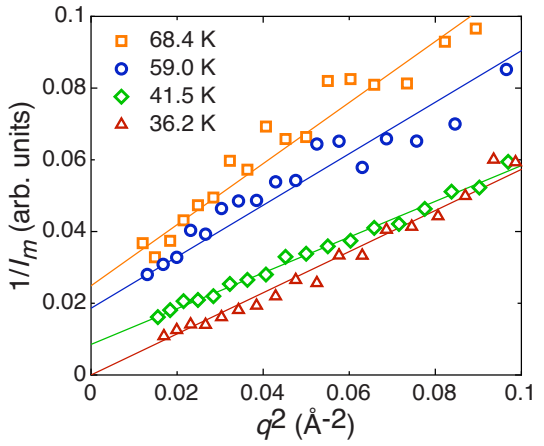

FIG. 7. (Color online) Inverse of the magnetic SANS intensity as a function of q^2 at 36.2, 41.5, 59.0, and 68.4 K (open triangles, diamonds, circles, and squares, respectively). For simplicity, mean values out of four q values has been represented. Straight lines are guides to the eyes.

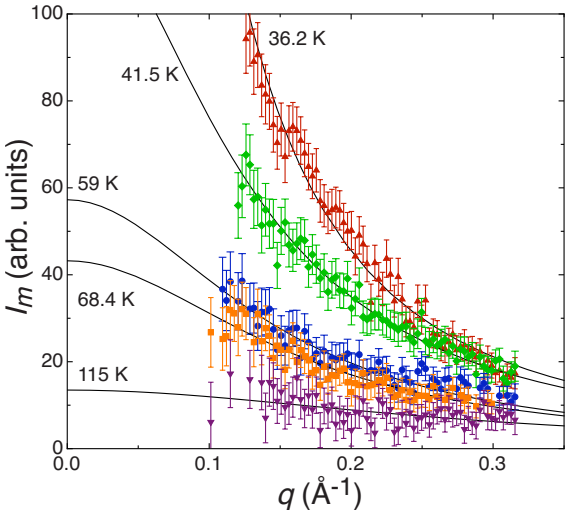

FIG. 8. (Color online) Magnetic SANS intensity as a function of q at selected temperatures: 36.2, 41.5, 59.0, 68.4, and 115.0 K. Full lines are fits of the isothermal data to a Lorentzian function as described in the text.

$$I_m = \frac{I_o}{q^2 + \frac{1}{\xi^2}}, \tag{1}$$

where ξ is the correlation length and I_o is a constant. This implies that the observed magnetic correlations have the Ornstein-Zernike form[60]

$$\langle M(0)M(r)\rangle = \frac{\exp(-r/\xi)}{r}. \tag{2}$$

Figure 8 shows selected $I_m(q)$ curves and their fits to a Lorentzian function for $ErCo_2$ in the paramagnetic phase for 1 T. From the fits, the quantitative values of I_o and ξ can be obtained. The temperature behavior of both magnitudes is represented in Fig. 9. As expected, I_o is constant at high temperatures and smoothly increases when cooling from T_f to the ordering transition. On the other hand, ξ experiences a continuous increase from high temperatures down to T_f. In the proximity of T_f, the correlation length reaches a plateau, at an almost constant value of $\sim 7 \pm 1$ Å. At lower temperatures, as the transition region is approached, ξ diverges due to the establishment of long-range order. For comparison, the evolution with the temperature of I_m for three different q values (q=0.12, 0.14, and 0.25 Å^{-1}) is also shown.

It is worth noting the relationship between the XMCD and SANS results, both at T_c and T_f. Figure 10 shows the evolution with temperature at H=1 T of the net magnetization per atom of the Co sublattice (m_{Co}) obtained from XMCD measurements and the correlation length obtained from the SANS analysis. Right at the ordering temperature, both ξ and the absolute value of m_{Co} experience an abrupt increase, showing that the establishment of long-range order coincides with the metamagnetic ordering transition of Co moments. On the other hand, the temperature region where ξ takes an almost constant value coincides with the change of sign of

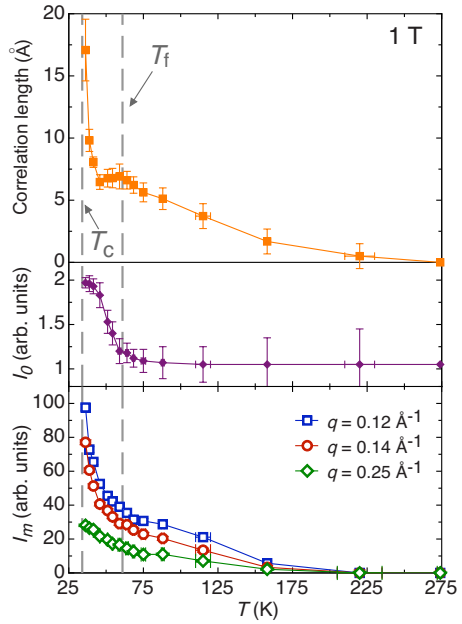

FIG. 9. (Color online) Upper and middle panels: ξ and I_o as a function of behavior at 1 T in the paramagnetic phase of $ErCo_2$ obtained from the fits of I_m to Eq. (1). Lower panel: I_m as a function of temperature at selected q values for $ErCo_2$ under an applied magnetic field of 1 T.

the net magnetization of the Co sublattice. This means that well within the paramagnetic phase, in the proximity of T_f, the magnetic clusters are already present. Moreover, Fig. 10 suggests that Co atoms have a very important role in the formation of the clusters, as the $\chi(T)$ measurements presented in the next section will demonstrate.

It is also interesting to carefully examine the temperature evolution of the magnetization of the Co sublattice in Fig. 10: at the ordering transition, the Co sublattice magnetization jumps from a value of $\sim 0.8\ \mu_B$/atom in the low-temperature site to a value of $\sim 0.2\ \mu_B$/atom, suggesting a transition from a low-temperature high-spin state to a high-temperature low-spin state at T_c. However, in contrast with the theoretical prediction by Liu and Altounian,[32] our results show that the

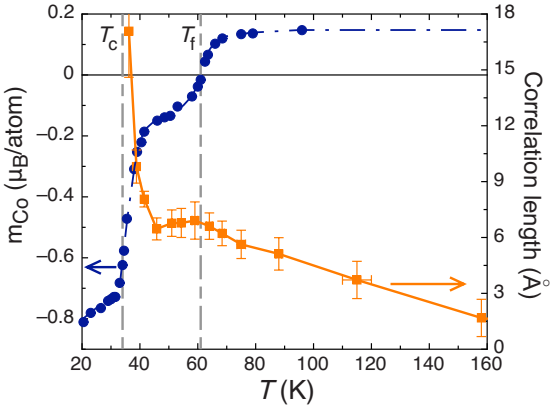

FIG. 10. (Color online) Correlation length (squares) and Co net magnetization per atom obtained from the XMCD measurements (circles) as a function of the temperature in $ErCo_2$ at 1 T.

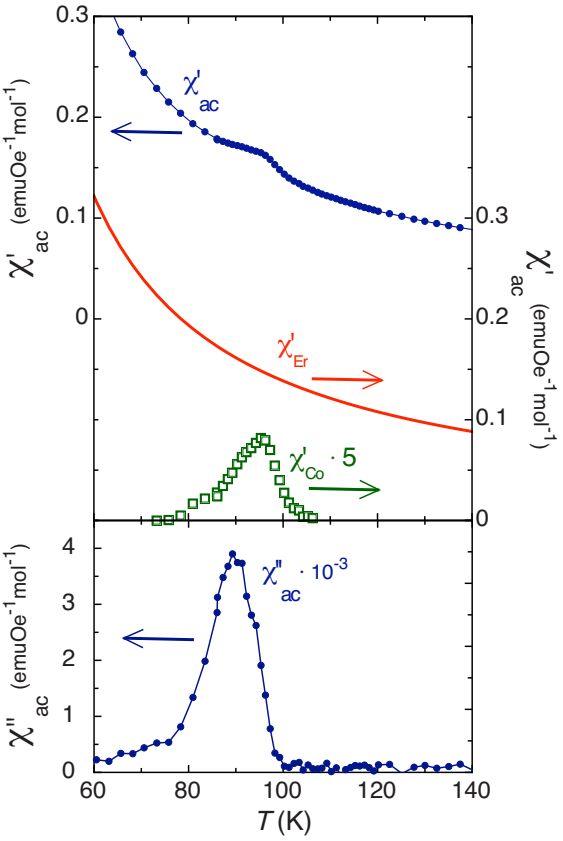

FIG. 11. (Color online) Paramagnetic susceptibility as a function of temperature at $H=0$ T in the compound $ErCo_2$. Full dots are the real (upper panel) and imaginary (lower panel) parts of the paramagnetic susceptibility. The continuous line represents the Er contribution (see the text for details). Empty squares are the Co contribution to the paramagnetic susceptibility.

low-spin state is stable up to temperatures well above the ordering temperature T_c.

C. Paramagnetic susceptibility

In order to further investigate the origin of this unusual magnetic arrangement in the compound $ErCo_2$, we have measured ac susceptibility as a function of temperature $[\chi(T)]$. The measurements were performed in a commercial SQUID Quantum Design magnetometer from 5 to 300 K with zero dc applied magnetic field. The ac excitation field has a magnitude of 4.5 Oe and a frequency of 100 Hz. We only present here the study performed at the paramagnetic phase. The real (χ', full dots in the upper panel) and imaginary (χ'', full dots in the lower panel) components of the paramagnetic ac susceptibility of $ErCo_2$ are shown in Fig. 11. Two contributions can be observed in χ': the expected T^{-1} dependence (Curie-Weiss law) and a small anomaly near $T=90$ K. This anomaly is by far more visible in χ'' raw data, where a peak of 20 K wide is present in the proximity of $T=90$ K, indicating an energy absorption process taking place in this temperature region.

If the region of the anomaly is excluded, χ' can be fitted to a Curie-Weiss law with an effective moment of 8.8 μ_B, both above and below the anomaly. This indicates that this contribution is due to paramagnetic Er moments. The fit is shown as a continuous line in Fig. 11. The difference of χ' and the fit to the Curie-Weiss law is a peak also shown in Fig. 11 (open squares), whose temperature, field, and frequency dependence has been thoroughly studied and will be the subject of a future work.[61] This contribution can be clearly ascribed to a relaxation Debye-like process from an adiabatic regime (at low temperature) to an isothermal one (at high temperature). As the process occurs in the paramagnetic phase, the isothermal susceptibility obeys a Curie-Weiss law with the temperature giving rise to the observed peak (as theoretically predicted in Ref. 62) instead of the typical steps reported for Debye processes in magnetically ordered phases.[63]

From the Curie-Weiss law for the isothermal susceptibility, the effective moment of the magnetic entities undergoing the relaxation process (μ_{eff}) can be obtained from

$$\chi_{eq} = \frac{C}{T - T_o} = \frac{N\mu_{\text{eff}}^2 \mu_B^2}{3k_B(T - T_o)}, \tag{3}$$

where N is the number of dynamic entities and $T_o=70$ K is the so-called Vogel-Fulcher temperature obtained from the fit of the relaxation time τ to the function $\tau(T) = \tau_0 \exp(Q/[k_B(T-T_o)])$.[64,65]

The obtained value, $\mu_{\text{eff}} \sim 20\ \mu_B$, is greater than any individual moment present in the system and thus can only be explained as the relaxation of a group of moments or cluster. Moreover, if we impose the cluster size obtained from the SANS experiments at T_f (7–8 Å), the clusters would include from 60 to 100 Co atoms and 30 to 50 Er atoms. This size is only compatible with a cluster effective moment of $\mu_{\text{eff}} \sim 20\ \mu_B$ if the clusters exclusively consist of Co low-spin moments. This result confirms the relationship between the inversion of the Co net moment and the formation of clusters derived from Fig. 10, i.e., the flipping of the Co moments must be a collective process.

IV. MAGNETIC PHASE DIAGRAM OF $ErCo_2$

Experimental results described in the previous section can be understood as the formation of Co magnetic clusters in the proximity of T_f minimizes the energy needed to flip the Co moments below T_f by reducing the average number of Co pairs aligned antiparallel. Therefore, the occurrence of Co magnetic clusters allows the negative Co magnetization (i.e., antiparallel to H_{appl}) at a temperature much higher than T_c. The ferrimagnetic arrangement between Co and Er within the paramagnetic phase is an experimental evidence from XMCD, while magnetic and thermodynamic measurements assure the lack of long-range order at T_f.[35] Moreover, SANS and ac susceptibility measurements confirm the existence of those magnetic clusters and the analysis of the whole set of results shows that the clusters consist of around 60–100 Co atoms.

Extending the experimental study to other applied magnetic fields and temperatures, the T-H flipping line where the Co sublattice magnetization is zero can be obtained, allowing

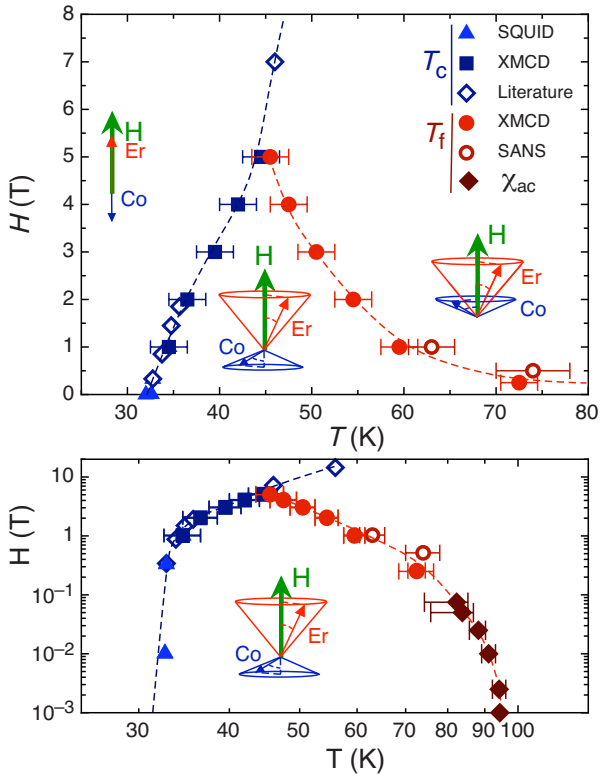

FIG. 12. (Color online) Magnetic phase diagram of the compound $ErCo_2$ in linear scale (upper panel) and logarithmic scale (lower panel). Squares and triangles are the critical temperature obtained from macroscopic magnetization measurements and XMCD, respectively. Open diamonds are selected values of T_c from the literature (Refs. 14 and 38). Full circles, open circles, and full diamonds are T_f obtained, respectively, from XMCD, SANS, and paramagnetic susceptibility measurements.

to determine the magnetic phase diagram of $ErCo_2$, which is presented in Fig. 12 in both linear scale (upper panel) and logarithmic scale (lower panel). Triangles and squares are the values of ordering temperature as obtained from macroscopic magnetization measurements and XMCD, respectively. Open diamonds are selected values of T_c from the literature.[14,38] Full circles are the temperatures (obtained from XMCD measurements) where the Co net magnetization becomes zero, i.e., T_f. The temperature dependence of both the magnetic SANS intensity and the correlation length allows to complete the phase diagram by determining T_f (open circles in Fig. 12) as the temperature region where ξ and I_m show a plateau. On the low magnetic field region, the phase diagram can be completed from the position of the anomaly in the paramagnetic susceptibility, which shifts to lower temperatures as a small magnetic field is applied (full diamonds, only shown in lower panel of Fig. 12).

The average antiparallel arrangement between the Co and the rare-earth sublattices in the paramagnetic phase was observed by Gignoux *et al.* by means of polarized neutron diffraction in other heavy rare-earth compounds of the RCo_2 family, in particular, in $TmCo_2$, $HoCo_2$,[22] and $TbCo_2$.[66] Gignoux *et al.* reported a change of sign of the Co sublattice magnetization for $TmCo_2$, taking place between 125 and 250 K (well above $T_c \sim 4$ K in $TmCo_2$). This change of sign of the Co sublattice in $TmCo_2$ was also observed by Hirosawa and Nakamura from ^{59}Co NMR experiments, but they do not give account of the temperature region where the change takes place.[67] Also in good agreement with our results, short-range magnetic correlations in the paramagnetic phase have been reported in $ErCo_2$ above T_c from the neutron diffraction by Pigorov *et al.*[68] and Podlesnyak *et al.*[69] and from the electrical resistivity by Garcia *et al.*[26] Moreover, Deportes *et al.*[70] evoked the existence of short-range magnetic order at temperatures four times higher than T_c in the ferromagnetic Laves phase compound $CeFe_2$, also pointing to the importance of *M-M* interactions in the paramagnetic phase of these intermetallic compounds. In this work, we have quantitatively characterized the short-range correlations in $ErCo_2$ as a function of temperature and field and soundly associated the existence of magnetic clusters with the antiparallel alignment of the separate magnetization of the Co and Er sublattices in the paramagnetic phase.

The magnetic phase diagram depicted in Fig. 12 clearly establishes the temperature and magnetic field region where the configuration of the Co and Er moments leads to a different paramagnetic phase in $ErCo_2$, which can adequately be coined by the term parimagnetic, derived from ferri- and paramagnetism. Schematic pictures of the magnetic arrangements are also shown in Fig. 12. At low temperatures, the typical ferrimagnetic structure is shown, i.e., Er and Co moments ordered in opposite senses along the easy axes. In the paramagnetic phase, the cones in Fig. 12 reflect the thermally disordered Er and Co magnetic moments with a net projection (and resulting magnetization) along the direction of the applied field. T_f separates the region where the Co cones are parallel ($T > T_f$) or antiparallel ($T < T_f$) to H_{appl}. Within the parimagnetic phase (i.e., $T_c < T < T_f$), if a picture of the magnetic moments would be taken at a given time, the "frozen" magnetic structure would resemble the one observed in a sperimagnetic structure, found in some amorphous magnetic compounds.[46] Of course, the nature of both phases is very different, as the parimagnet in $ErCo_2$ is a thermally disordered magnetic phase (in space and probably in time) held by an ordered atomic structure, while the sperimagnet maintains its magnetic arrangement stable in time, but it is supported by an amorphous structure.

V. CONCLUSIONS

The XMCD, SANS, and $\chi(T)$ measurements on $ErCo_2$ have been analyzed in order to shed light on the understanding of the properties of the Co sublattice in the paramagnetic phase of this compound. The XMCD measurements show an inversion of the Co magnetization at a temperature T_f well above the ferrimagnetic transition. To flip the orientation of a single Co moment, it is necessary to overcome the Co-Co exchange interaction H_{CoCo}. Therefore, even in the paramagnetic phase, it is not energetically favorable that Co moments flip individually, i.e., the reversal of the Co magnetization is only possible with the formation of magnetic clusters, in which Co magnetic moments play an important role. Indeed, our SANS measurements confirm the presence of these mag-

netic clusters and we have characterized its magnetic correlation length as a function of the temperature and the applied field. The magnetic susceptibility measurements show the existence of a relaxation process in the paramagnetic phase of the compound $ErCo_2$. A detailed analysis of the $\chi(T)$ curve allows us to show that the entities undergoing the relaxation process are clusters formed by 60–100 low-spin Co moments. We have shown that the reversal of the Co moments at T_f can only take place if the flipping is a collective behavior, as the strongest interaction in the system is the Co-Co exchange. The whole experimental study has allowed us to determine the existence of a finite region of the phase diagram, at temperatures above the magnetic ordering transition, in which Co net moment is inverted with respect to the Er one, which we have coined as parimagnetic.

It would be interesting to investigate if such a parimagnetic phase is a particular feature of $ErCo_2$. In principle, a similar behavior should be expected in the other ferrimagnetic RCo_2 compounds, such as $TmCo_2$, $HoCo_2$, $DyCo_2$, and $TbCo_2$. Moreover, this could be a more general feature of ferrimagnetic materials, and it seems interesting to study whether a parimagnetic phase takes place just above the magnetic ordering transition. In principle, one would expect that the occurrence of a parimagnetic region is favored in those ferrimagnets in which the various magnetic moments involved are very different in magnitude.

ACKNOWLEDGMENTS

We acknowledge the Spanish CICYT Research Project No. MAT2005-02454, the FEDER program, and the Aragonese CAMRADS research group. We thank F. Luis, E. García-Matres, A. Heinemann, A. Wiedenmann, R. Ibarra, and P. A. Algarabel for fruitful discussions, N. Plugaru and M. J. Pastor for sample preparation, S. P. Cramer for the use of a cryomagnet at the ALS, and J. Bartolomé for careful reading of the manuscript. J.H.A. acknowledges Conrado Rillo for financial support.

*julia.herrero@unizar.es; URL: http://fmc.unizar.es/

[1] E. Burzo, A. Chelkowski, and H. R. Kirchmayr, in *Magnetic Properties of Metals: Compounds Between Rare Earth Elements and 3d, 4d or 5d Elements*, edited by H. P. J. Wijn, Landolt-Börnstein, New Series, Group III, Vol. 19d2 (Springer, Berlin, 1990).

[2] H. Yamada, J. Inoue, K. Terao, S. Kanda, and M. Shimizu, J. Phys. F: Met. Phys. **14**, 1943 (1984).

[3] J. J. M. Franse and R. J. Radwanski, *Magnetic Properties of Binary Rare-Earth 3d-Transition-Metal Intermetallic Compounds* (Elsevier, Amsterdam, 1993), Vol. 7, Chap. 5.

[4] N. H. Duc and P. E. Brommer, in *Handbook on Magnetic Materials*, edited by K. H. J. Buschow (North-Holland, Amsterdam, 1999), Vol. 12, Chap. 3, p. 259.

[5] E. Gratz and A. S. Markosyan, J. Phys.: Condens. Matter **13**, R385 (2001).

[6] R. Hauser, E. Bauer, and E. Gratz, Phys. Rev. B **57**, 2904 (1998).

[7] S. Khmelevskyi and P. Mohn, J. Phys.: Condens. Matter **12**, 9453 (2000).

[8] O. Syshchenko, T. Fujita, V. Sechovsky, M. Divis, and H. Fujii, J. Magn. Magn. Mater. **226-230**, 1062 (2001).

[9] T. Goto, K. Fukamichi, T. Sakakibara, and H. Komatsu, Solid State Commun. **72**, 945 (1989).

[10] H. Yamada, Phys. Rev. B **47**, 11211 (1993).

[11] N. H. Duc and T. Goto, in *Handbook on Physics and Chemistry of the Rare Earths*, edited by K. A. Gschneidner, Jr. and L. Eyring (North-Holland, Amsterdam, 1999), Vol. 26, Chap. 171.

[12] M. Ohta, K. Fukamichi, A. Fujita, H. Saito, and T. Goto, J. Alloys Compd. **394**, 43 (2005).

[13] H. Wada, S. Tomekawa, and M. Shiga, J. Magn. Magn. Mater. **196-197**, 689 (1999).

[14] A. Giguere, M. Foldeaki, W. Schnelle, and E. Gmelin, J. Phys.: Condens. Matter **11**, 6969 (1999).

[15] N. A. de Oliveira, P. J. von Ranke, M. V. Tovar Costa, and A. Troper, Phys. Rev. B **66**, 094402 (2002).

[16] N. H. Duc and D. T. K. Anh, J. Magn. Magn. Mater. **242-245**, 873 (2002).

[17] J. Herrero-Albillos, F. Casanova, F. Bartolome, L. M. Garcia, A. Labarta, and X. Batlle, J. Magn. Magn. Mater. **301**, 378 (2006).

[18] D. Gignoux, D. Givord, F. Givord, W. C. Koehler, and R. M. Moon, Phys. Rev. B **14**, 162 (1976).

[19] E. Burzo, Phys. Rev. B **6**, 2882 (1972).

[20] D. Bloch and R. Lemaire, Phys. Rev. B **2**, 2648 (1970).

[21] J. Voiron, A. Berton, and J. Chaussy, Phys. Lett. **50A**, 17 (1974).

[22] D. Gignoux, F. Givord, and W. C. Koehler, Physica B & C **86-88**, 165 (1977).

[23] L. Nordstrom, M. S. S. Brooks, and B. Johansson, J. Magn. Magn. Mater. **104-107**, 1378 (1992).

[24] M. I. Bartashevich, H. Aruga Katori, T. Goto, H. Wada, T. Maeda, T. Mori, and M. Shiga, Physica B **229**, 315 (1997).

[25] P. de la Presa, S. Muller, A. F. Pasquevich, and M. Forker, J. Phys.: Condens. Matter **12**, 3423 (2000).

[26] F. Garcia, M. R. Soares, and A. Y. Takeuchi, J. Magn. Magn. Mater. **226-230**, 1197 (2001).

[27] A. L. de Oliveira, N. A. de Oliveira, and A. Troper, J. Magn. Magn. Mater. **270**, 208 (2004).

[28] J. Woo, Y. Jo, H. C. Kim, A. Pigorov, J. G. Park, H. C. Ri, A. Podlesnyak, J. Schefer, T. Strassle, and A. Teplykh, Physica B **329**, 653 (2003).

[29] R. Moon, W. C. Koehler, and J. Farrell, J. Appl. Phys. **36**, 978 (1965).

[30] H. Imai, H. Wada, and M. Shiga, J. Magn. Magn. Mater. **140-144**, 835 (1995).

[31] O. Syshchenko, T. Fujita, V. Sechovsky, M. Divis, and H. Fujii, J. Alloys Compd. **317-318**, 438 (2001).

[32] X. B. Liu and Z. Altounian, J. Phys.: Condens. Matter **18**, 5503 (2006).

[33] J. Rodriguez-Carvajal, in Abstracts of the Satellite Meeting on Powder Diffraction of the XV Congress of the IUCr, Toulouse, France, 1990 (unpublished), p. 127.

[34] J. Rodriguez-Carvajal, Physica B **192**, 55 (1993).

[35] J. Herrero-Albillos, F. Bartolome, L. M. Garcia, F. Casanova, A.

Labarta, and X. Batlle, Phys. Rev. B **73**, 134410 (2006).
[36] U. Atzmony and G. Dublon, Physica B & C **86-88**, 167 (1977).
[37] R. M. Moon, W. C. Koehler, H. R. Child, and L. J. Raubenheimer, Phys. Rev. **176**, 722 (1968).
[38] F. Givord and J. S. Shah, C. R. Acad. Sci. III **247**, 923 (1972).
[39] O. Syshchenko, T. Fujita, V. Sechovsky, M. Divis, and H. Fujii, Phys. Rev. B **63**, 054433 (2001).
[40] N. H. Duc, D. T. K. Anh, and P. E. Brommer, Physica B **319**, 1 (2002).
[41] J. Herrero-Albillos, F. Casanova, F. Bartolome, L. M. Garcia, X. Batlle, and A. Labarta, J. Magn. Magn. Mater. **290-291**, 682 (2005).
[42] A. T. Young, V. Martynov, and H. A. Padmore, J. Electron Spectrosc. Relat. Phenom. **101-103**, 885 (1999).
[43] A. T. Young *et al.*, Nucl. Instrum. Methods Phys. Res. A **467-468**, 549 (2001).
[44] T. Funk, A. Deb, S. J. George, H. Wang, and S. P. Cramer, Coord. Chem. Rev. **249**, 3 (2005).
[45] J. B. Goedkoop, Ph.D. thesis, Katholieke Universiteit te Nijmegen, 1989.
[46] S. Pizzini, L. M. Garcia, A. Fontaine, J. P. Rueff, J. Vogel, R. M. Galera, J. B. Goedkoop, N. B. Brookes, G. Krill, and J. P. Kappler, J. Electron Spectrosc. Relat. Phenom. **86**, 165 (1997).
[47] C. T. Chen, Y. U. Idzerda, H.-J. Lin, N. V. Smith, G. Meigs, E. Chaban, G. H. Ho, E. Pellegrin, and F. Sette, Phys. Rev. Lett. **75**, 152 (1995).
[48] J. P. Liu, Ph.D. thesis, University of Amsterdam, 1994.
[49] N. H. Duc and D. Givord, J. Magn. Magn. Mater. **151**, L13 (1995).
[50] V. Y. Irkhin, J. Phys.: Condens. Matter **14**, 6865 (2002).
[51] Y. Oner, E. Alveroglu, and O. Kamer, J. Alloys Compd. **424**, 60 (2006).
[52] C. Dewhurst, GRASP, Institut Laue Langevin, Grenoble, France.
[53] J. M. De Teresa, P. A. Algarabel, C. Ritter, J. Blasco, M. R. Ibarra, L. Morellon, J. I. Espeso, and J. C. Gomez-Sal, Phys. Rev. Lett. **94**, 207205 (2005).
[54] N. Veglio, F. J. Bermejo, J. Gutierrez, J. M. Barandiaran, A. Pena, M. A. Gonzalez, P. P. Romano, and C. Mondelli, Phys. Rev. B **71**, 212402 (2005).
[55] C. Ritter, M. R. Ibarra, J. M. De Teresa, P. A. Algarabel, C. Marquina, J. Blasco, J. García, S. Oseroff, and S.-W. Cheong, Phys. Rev. B **56**, 8902 (1997).
[56] J. E. Greedan, N. P. Raju, A. Maignan, C. Simon, J. S. Pedersen, A. M. Niraimathi, E. Gmelin, and M. A. Subramanian, Phys. Rev. B **54**, 7189 (1996).
[57] S. V. Grigoriev, S. V. Maleyev, A. I. Okorokov, H. Eckerlebe, and N. H. van Dijk, Phys. Rev. B **69**, 134417 (2004).
[58] J. M. De Teresa *et al.*, Phys. Rev. B **65**, 100403 (2002).
[59] S. K. Burke, R. Cywinski, and B. D. Rainford, J. Appl. Crystallogr. **11**, 644 (1978).
[60] H. E. Stanley, *Introduction to Phase Transitions and Critical Phenomena* (Clarendon, Oxford, 1971).
[61] J. Herrero-Albillos, F. Bartolomé, and L. M. García (unpublished).
[62] J. L. Garcia-Palacios and D. Zueco, J. Phys. A **39**, 13243 (2006).
[63] L. M. García, J. Bartolomé, F. J. Lázaro, C. de Francisco, and J. M. Muñoz, Phys. Rev. B **54**, 15238 (1996).
[64] H. Vogel, Phys. Z. **22**, 645 (1921).
[65] G. Fulcher, J. Am. Ceram. Soc. **8**, 339 (1925).
[66] D. Gignoux and F. Givord, J. Phys. F: Met. Phys. **9**, 1409 (1979).
[67] S. Hirosawa and Y. Nakamura, J. Appl. Phys. **53**, 2069 (1982).
[68] A. Pirogov, A. Podlesnyak, T. Strassle, A. Mirmelstein, A. Teplykh, D. Morozov, and A. Yermakov, Appl. Phys. A: Mater. Sci. Process. **74**, s598 (2002).
[69] A. Podlesnyak, T. Strassle, J. Schefer, A. Furrer, A. Mirmelstein, A. Pirogov, P. Markin, and N. Baranov, Phys. Rev. B **66**, 012409 (2002).
[70] J. Deportes, D. Givord, and K. R. A. Ziebeck, J. Appl. Phys. **52**, 2074 (1981).